# Porous elastic composite scaffolds based on enzymatically synthesized poly(glycerol adipate) and bioglass: the effect of L-lysine diisocyanate content on crosslinking degree and mechanical properties

**Michał Grzymajło[1*], Anna Krokos[1], Konrad Szustakiewicz[1*], Magdalena Kobielarz[2], Ewelina Ortyl[1], Anna Nikodem[2], Lidia Ciołek[3], Monika Biernat[3], Sylwia Rodziewicz-Motowidło[4], Artur Oziębło[3,5] , Małgorzata Gazińska[1]**

[1] *Department of Polymer Engineering and Technology, Faculty of Chemistry, Wrocław University of Science and Technology (WUST), Wyb. Wyspiańskiego 27, 50-370 Wrocław, Poland*

**corresponding authors: michal.grzymajlo@pwr.edu.pl, malgorzata.gazinska@pwr.edu.pl*

[2] *Department of Mechanics, Materials and Biomedical Engineering, Faculty of Mechanical Engineering, Wrocław University of Science and Technology (WUST), Wyb. Wyspiańskiego 27, 50-370 Wrocław, Poland*

[3] *Biomaterials Research Group, Ceramic and Concrete Division in Warsaw, Łukasiewicz Research Network Institute of Ceramics and Building Materials, Postępu 9, 02-676 Warsaw, Poland*

[4] *Faculty of Chemistry, University of Gdańsk, Wita Stwosza 63, 80-308 Gdańsk, Poland*

[5] *Mossakowski Medical Research Institute, Polish Academy of Sciences, A. Pawińskiego 5, 02-106 Warsaw*

## ABSTRACT

**In this research, poly(glycerol adipate) prepolymer (pPGA) was synthetized using enzymatic polymerization of divinyl adipate (DVA) and glycerol in reaction carried out in the presence of *Candida Antarctica* enzyme. The pPGA was then solved in 1,4-dioxane and mixed with L-lysine diisocyanate (LDI), bioglass, pourged into mold with sodium chloride, cured and freeze-dried. LDI has a dual function in the system: it is a cross-linking agent and also a bioactive agent that is chemically bound to the scaffold. Three types of porous composite scaffolds having 20 wt.% of bioglass and different cross-linking degree (25, 50 and 100 mol% of LDI) were investigated. The scaffolds were**

**characterized by means of porosity, density, SEM. All tested materials were subjected to a quasi - static compression test. Each material was compressed 10 times. It was shown that the materials exhibited a return to their original shape even with a large compression strain of 90%. An imaging study of the scaffolds before and after compression was conducted using computed tomography (CT). The CT study showed that the resulting materials were not significantly mechanically damaged in the multi - compression process.**

**Keywords:** poly(glycerol adipate), thermally induced phase separation, scaffolds, mechanical properties, LDI, chemical crosslinking, bioglass, composite materials

## 1. INTRODUCTION

In recent years enzymatic synthesis has become an interesting, popular and greener method for polymerization [1,2]. Enzymatic synthesis seems to be beneficial in the context of reaction conditions (low temperature), bio-based, heavy metal-free catalyst with low toxicity as well as products properties – usually enzymatically synthesized polymers have good linearity [2,3].

Poly (glycerol adipate) (PGA) belongs to a group of promising biodegradable polyesters that can be obtained in enzymatic synthesis in the presence of Novozym 435 that consists of CAL-B (*Candida Antarctica Lipase B*) [4,5]. PGA have several potential biomedical applications, i.e. as carrier in drug delivery systems [6,7], especially popular to produce sophisticated nanoparticles as a targeted and controlled active agent release[8].

As a monomer for obtaining PGA, divinyl adipate (DVA) is most often used along with glycerin [9,10]. Due to the presence of Lipase B, the DVA polymerization reaction is often carried out under mild conditions, i.e. at relatively low temperatures not exceeding 80°C [10–12]. The result is a polymer with a relatively low molecular weight generally not exceeding a few thousand Daltons [4,11].

The literature also contains information on chemical modification of PGA using i.e. phenylalanine or trypthophan [4] and others. These modifications affect the branching degree, molecular weigth distriubution which affect physicochemical properties of the obtained polymer [5]. The presence of free hydroxyl groups in the PGA chain allows its numerous chemical modifications. The modification reaction of PGA with acid chlorides containing different hydrocarbon lengths leads to products with different properties, such as $T_g$. PGA derivatives of this type can undergo a self-organization process to form nanoparticles with high homogeity, the size of which depends on the degree of chloride substitution and the length of the chloride chain used for modification [13,14].

A well-established strategy for post-polymerization modification of pPGA is the Steglich esterification reaction. This reaction is carried out under mild conditions, often at room temperature, using a N,N'-dicyclohexylcarbodiimide (DCC) as coupling agent and 4-dimethylaminipyridine (DMAP) as catalyst. A few examples of this type of reaction described in the literature are modifications of PGA with: N-acyl-tryptophan, N-acyl-tyrosine, N-acyl phenylalanine and methotrexate [12,15,16]

Tissue engineering is now increasingly considering the use of so-called scaffolds (artificially created three-dimensional structures that support cells). Scaffolds are used to repair damaged tissues [17]. There are several known methods for obtaining polymer scaffolds for regenerative medicine applications. The most popular scaffold fabrication techniques include electrospinning [18–20], solvent casting and particle leaching [21], gas foaming [22], solid free form fabrication [23], thermally induced phase separation (TIPS) [24] and 3D printing [25–27]. The mentioned techniques allow to obtain scaffolds mainly from biopolymers based materials [28].

Using the TIPS technique, it is possible to obtain a scaffold with a three-dimensional structure, high porosity, even at a level over 90% (total porosity). The technique allows

controlling the size of pores [29], and also makes it possible to introduce additives, such as fillers in excess of 50% by weight in the system, while maintaining a low density of the material [30]. Systems based on poly(glyceryl adipate) or poly(glyceryl sebacate), however, require the use of a thermal [31], chemical crosslinking using i.e. hexamethylene diisocyanate (HDI) [32] so that a dimensionally stable scaffold can be obtained. There are also reports in the literature of chemical modification of PGA combined with UV crosslinking [33]. PGA derivatives or cross-linking can be obtained by functionalizing the side hydroxyl groups present along the main polymer chain [11].

Often, polymer scaffolds contain other components besides the polymer itself, such as fillers in the form of apatite ceramics (hydroxyapatite, Beta-TCP, Bio Glass) [34]. The purpose of introducing these fillers into the system is to provide osteoconductivity, and such scaffolds themselves are used in bone tissue engineering [35,36].

Polymer-filler composite systems often also contain bioactive additives, the most popular of which are L-lysine and L-arganine. L-lysine belongs to the group of amino acids and is used in osteoporosis fracture healing [37]. L-lysine can be introduced into the polymer-filler system in several ways, including: filler chemical functionalization [38], filler physical impregnating [29] or adding it directly as a second filler [39].

In the present work, three-dimensional porous scaffolds were produced based on enzymatically obtained PGA, which was doped with bio-glass and chemically cross-linked using L-lysine diisocyanate (LDI). LDI acts as a crosslinking agent but also ensures the potential bioactivity of the material. The effect of LDI content and bioglass on the physicochemical properties and compression parameters of the obtained composites was studied.

## 2. EXPERIMENTAL SECTION

### 2.1 Materials

In this research, divinyl adipate (Tokyo Chemical Industry), Glycerol (>99,5%, Sigma Aldrich®), Novozym 435 (STREM Chemicals), L-lysine ethyl ester diisocyanate (LDI, 97%, AlfaAesar™), 1,4-dioxane (>99%, Honeywell), sodium chloride having grain size of 500-600μm (Avantor, Poland) were used.

### 2.2 Bioglass synthesis

The P5Sr2 Bioglass (BG) was obtained from Institute of Ceramics and Building Materials (Warsaw, Poland) and detailed preparation was described before [40]. The BG belongs (based on) to the $CaO$-$SrO$-$SiO_2$-$P_2O_5$ system was produced using the sol-gel method. After the reaction (of substrates) mixtures were transformed from the sol into a gel and dried in an electric furnace at a temperature of 650°C. The obtained coarse-grained powders were initially ground in a mechanical mortar and then milled in a rotary-vibration mill.

### 2.2 pPGA synthesis and foam formation

The pPGS synthesis was carried out in a 250 $cm^3$ double-necked glass round bottom flask equipped with a reflux condenser and thermometer. In the vessel were placed 62.5 mmol each of DVA and glycerol, 25 $cm^3$ of THF previously dried over molecular sieves as the reaction medium, and 0.55 g of Novozyme 435 as the enzyme catalyst. The flask above the reaction mixture was purged with nitrogen and then heated The synthesis was carried out at temperature of 40˚C. The mixture was homogenized for 24 h with a magnetic dipole at 250 rpm. After the reaction was stopped, Novozym 435 was drained on a paper filter, and THF and low-molecular-weight volatile products were removed on a rotary vacuum evaporator. In order to deactivate lipase that could be eluted from the acrylic carrier, the product was placed in a forced-air dryer for 1 h at 95˚C. The product was finally dried in a vacuum dryer for 72 h at 40˚C.

PGA/BG scaffolds were fabricated in several steps. Initially, 20 wt. % solution of pPGS-LDI in 1,4-dioxane was prepared. The LDI content corresponds to react of 25 wt.%, 50 wt.% or 100 wt.% of hydroxyl groups from PGA (according to the scheme showed in Figure 1). Both scaffolds were also prepared with 20 wt.% of BG and sodium chloride (with grain size of 500-600 µm). The scaffolds were then frozen (24h, -40°C ), freeze-dried (24h, 10Pa), cross-linked (24h, 60°C), then the sodium chloride was washed off and finally the scaffolds were dried (72h, 40°C). All the samples compositions are summarized in table 1. The scaffold preparation procedure is shown in Figure 2.

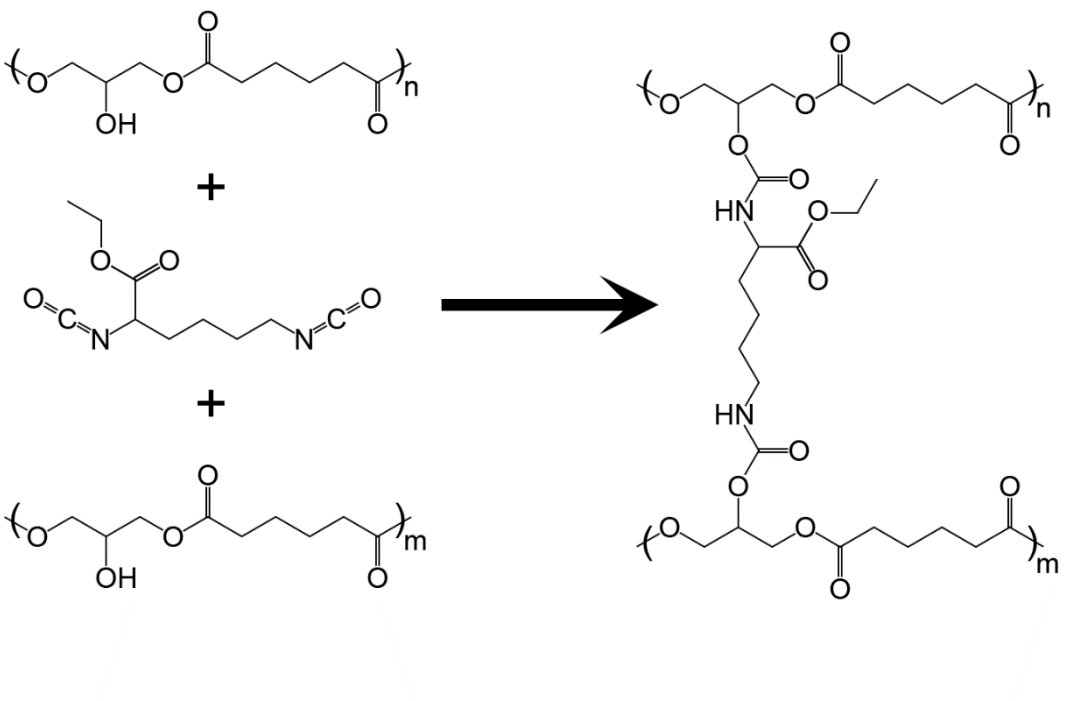

**Figure 1.** pPGA cross-linking with LDI scheme.

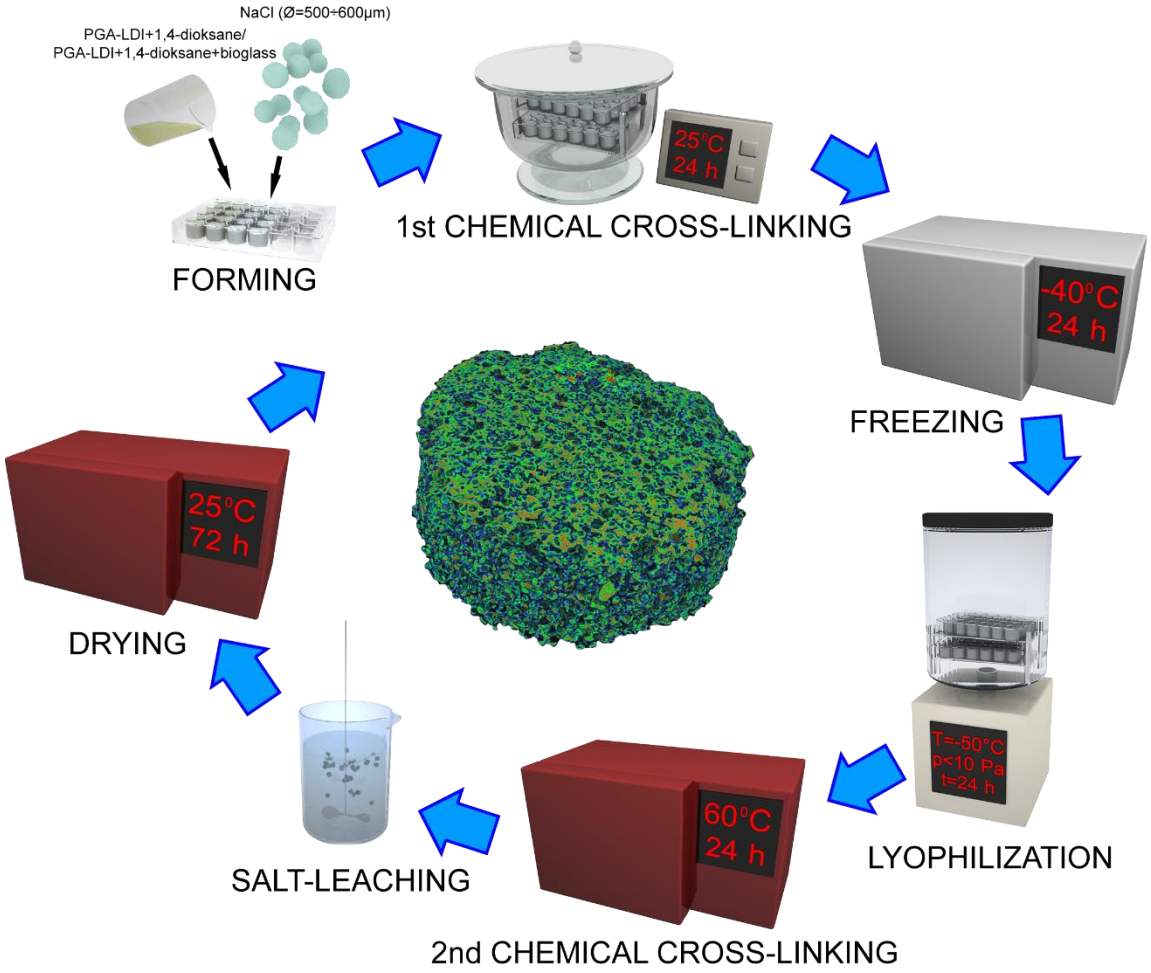


**Figure 2.** Scaffold preparation procedure

**Table 1.** Samples designation

| Sample | LDI content in cross-linked PGA [mol] | PGA content [wt.%] | Bioglass content [wt.%] |
|---|---|---|---|
| PGA25 | 25 | 100 | - |
| PGA25/BG | 25 | 80 | 20 |
| PGA50 | 50 | 100 | - |
| PGA50/BG | 50 | 80 | 20 |
| PGA100 | 100 | 100 | - |
| PGA100/BG | 100 | 80 | 20 |

## 2.5 Physicochemical properties of the scaffolds

### Particle size distribution measurements

The particle size analysis was performed using a Malvern Instruments 2000–laser graining analyzer using the low-angle laser light scattering (LALLS) method. The device used allowed for examining the grain size in a wide range from 0.1 μm to 2000 μm with an error of 0.5%. The resulting characteristic values dv(0.1), dv(0.5) and dv(0.9) are particle sizes below which there is respectively 10 vol.%, 50 vol.%. and 90 vol.% sample population.

**Attenuated Total Reflectance-Fourier Transform Infrared Reflectance (FTiR/ATR)**

Attenuated Total Reflectance-Fourier Transform Infrared Reflectance spectra (FTIR/ATR) was used to track the progress of PGA crosslinking reaction using LDI. FTIR/ATR spectra were recorded with Nicolet iZ10 spectrometer (Thermo Scientific, Waltham, MA, USA) equipped with Smart iTR™ diamond ATR accessory. The spectra were acquired with a resolution of 4 $cm^{-1}$ in the range of 4000 – 550 $cm^{-1}$ (32 co-added scans).

**Thermogravimetry (TGA)**

TGA measurements were performed utilizing the TGA/DSC1 Mettler Toledo system to investigate thermal stability of obtained materials. Samples were heated at a 10°C/min in the temperature range from 25°C to 900°C under 60 $cm^3$/min of nitrogen flow.

**Differential scanning calorimetry (DSC)**

To establish a glass transition temperature of PGA, a DSC method was used. The measurement were carried out using DSC1 STARe Differential Scanning Calorimeter System from Mettler-Toledo. The measurements was carried out in the temperature range of -50 to 70°C with the heating/cooling rate 10 K/min. Samples were measured in aluminum pans under a constant nitrogen purge (60 ml/min). First cooling and second heating thermographs were used for analysis.

**Scaffolds (foams) micro-imaging (SEM)**

Morphologies of foam scaffolds the PGAs and PGA/BG systems, also after compression tests, were characterized by scanning electron microscopy (SEM) (Phenom ProX; Thermo

Scientific). The samples were sectioned on a cryostat (Hyrax C50, Zeiss) at -25°C to reveal the internal structure of foams, especially pores' shape, dimensions and arrangement. The samples were mounted on microscope stubs using double-sided adhesive carbon tape.

**Quasi - static compression tests**

Mechanical tests were carried out using an Instron 5966 universal testing machine, equipped with a 1 kN load cell and a set of compression analysis tables. All tests were carried out on cylindrical shape scaffolds with a diameter of 15.4 mm and a height of 4 mm. In order to capture the actual height of the shapes, the measurement was started at the original pivot of the top table equal to 5.0 mm, and the onset of preload equal to 0.05 N was defined as the beginning of the measurement. The results were recorded in Bluehill 3 software. The mechanical properties of the static compression test were determined at a compression speed of 1 mm / min. and a maximum strain was being read at 90% of deformation.

In addition, cyclic (fatigue) tests were carried out. When the preload was reached, an initial point was determined, and the scaffold was compressed at a speed of 10 mm/min to the target strain (30, 60, or 90%). Immediately after it was reached, the top table was returned to the starting point at the same speed. The entire cycle was repeated 10 times, so 10 local maxima were recorded.

**Microtomography (µCT)**

To examine microstructural properties, foam specimens were scanned using a microtomography (SkyScan 1172, Bruker, Kontich, Belgium). Samples were scanned using no filter, with a resolution of 9 µm, 180-degree scanning range. An X-ray lamp intensity of 222 µA, voltage energy of 44 kV, rotation step of 0,25º and exposure time of 500 ms was used. After the image reconstruction (NRecon, Bruker), cylindrical volumes of interest (VOIs) were

created within each foam. The created VOIs had a diameter of 10 mm and a height of 3.5 mm. Analysis of the microstructural parameters (CtAn, Bruker) was carried using three-dimensional parameters describing the foam porosity, such as: total porosity (Po(tot) [%]), open porosity (Po(op) [%]), closed porosity (Po(cl) [%]), open and closed pores volume (Po.V(op), Po.V(cl) [$mm^3$]) pore size (volume- equivalent sphere diameter, ESDv [µm]), major pore diameter (Maj.Dm [µm]), sphericity (Sph [-]).

## 2. RESULTS AND DISCUSSION

### 2.1. PGS/BG scaffolds properties

Table 2 contains the results of porosity, density and water sorption for the PGA/BG systems having different degree of cross-linking. It can be seen that materials containing BG are characterized by higher water sorption and porosity as compared to corresponding samples without BG (porosity of BG filled materials is 2-3% higher compared to corresponding non filled material while water sorption is higher by 40 to150% for filled systems as compared to references). An increase in the degree of cross-linking leads to an increase in the porosity of the scaffolds reaching porosity over 90% for PGA50/BG and PGA100/BG samples. The density of the PGA/BG composite is comparable to that of PGA having the same degree of cross-linking. However, the degree of cross-linking clearly influences the density of the material. For systems having a degree of cross-linking of 25%, the density is 0,154-0,163 $g/cm^3$, for systems having a degree of cross-linking of 50%, the density is 0,132-0,135 $g/cm^3$, while for samples having the highest degree of cross-linking, values of 0,122-0,127 $g/cm^3$ were obtained. The porosity results indicate that the higher the degree of – crosslinking, the lower the density of the obtained scaffolds. The results show that with a higher degree of cross-linking, the structure is much more dimensionally stable and does not collapse, thus reducing its density.

Water absorption is higher for samples containing bio-glass and does not depend on the degree of cross-linking. The reduction in water absorption of filled and most cross-linked specimens leads to assume that there is an optimal degree of cross-linking that guarantees the highest water absorption.

**Table 2.** Physical properties of PGA scaffolds

| Sample | Scaffold density [g/cm$^3$] | Scaffold porosity [volume %] | Water sorption [wt. %] |
|---|---|---|---|
| PGA25 | 0,163 +/- 0,008 | 85,2 +/- 0,8 | 710 +/- 20 |
| PGA25/BG | 0,154 +/- 0,006 | 88,9 +/- 0,4 | 810 +/- 20 |
| PGA50 | 0,135 +/- 0,006 | 87,7 +/- 0,6 | 780 +/- 20 |
| PGA50/BG | 0,132 +/- 0,006 | 90,4 +/- 0,7 | 930 +/- 20 |
| PGA100 | 0,122 +/- 0,005 | 88,9 +/- 0,4 | 810 +/- 20 |
| PGA100/BG | 0,127 +/- 0,006 | 90,8 +/- 0,5 | 850 +/- 20 |

## 2.2 Scaffolds structure and morphology (SEM)

Figures 3 and 4 show SEM images of chosen scaffolds cross sections before compression testing (Figure 3) and after compression (Figure 4). During testing, samples were compressed by 90%. The photos show cross sections only for selected materials.

Figure 3A shows a view of the pores and walls of the PGA25 scaffold, while Figure 3C shows the PGA50. Large pores with an estimated size of about 500 micrometers can be seen, which were formed by leaching of sodium chloride grains. Also, in both samples are small pores visible with a size of a dozen or so micrometers from the freeze-drying process.

Figures 3B and 3D feature scaffolds containing 25wt.% bio-glass and differing in the degree of cross-linking (25 and 50%, respectively). The bio-glass is located in the walls of the scaffolds. The walls of the obtained PGA based materials have a thickness of 30 to over 150 μm and are much thicker compared to the scaffolds obtained from PLLA [26] or PCL [35]. This effect is directly related to the concentration of polymer used for scaffolds preparation. In the

case of PGA scaffolds, the concentration of pPGS pre-polymer in the solution from which the materials were made was 20 wt. %, while for PLLA it was only 2.5 wt. % and for scaffolds made from PCL, the concentration of polymer in solution was 10 wt. %.

SEM images revealed slightly or lacked visible effects of compression onto the internal structure of foams (comparison of Figure 3 with Figure 4). Walls of pores were intact independently of foams' type. Slight defects were detected only for loose (unconnected) walls of pores for PGA50/BG (Figure 4D) as the bottom of pores. In the cross-sections of pores' walls, decohesions between polymer and bioglass were not present (Figure 4D`). Hence the risk of uncontrolled release of bioglass particles was absent. The level of load damping without significant changes in the foam structure is very high.

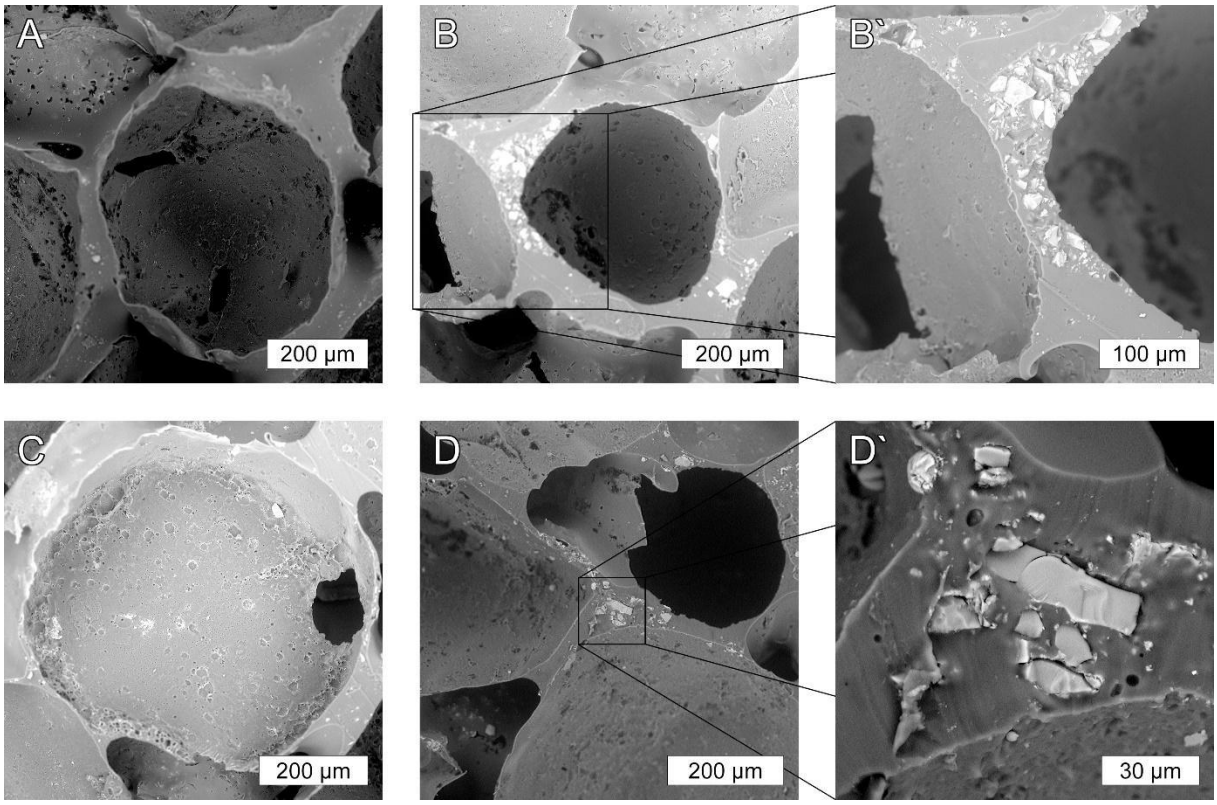


**Figure 3.** SEM images of foam scaffolds based on A) PGA25, B) PGA25/BG, B'PGA25/BG walls, C) PGA50, D) PGA50/BG and D` PGA50/BG walls

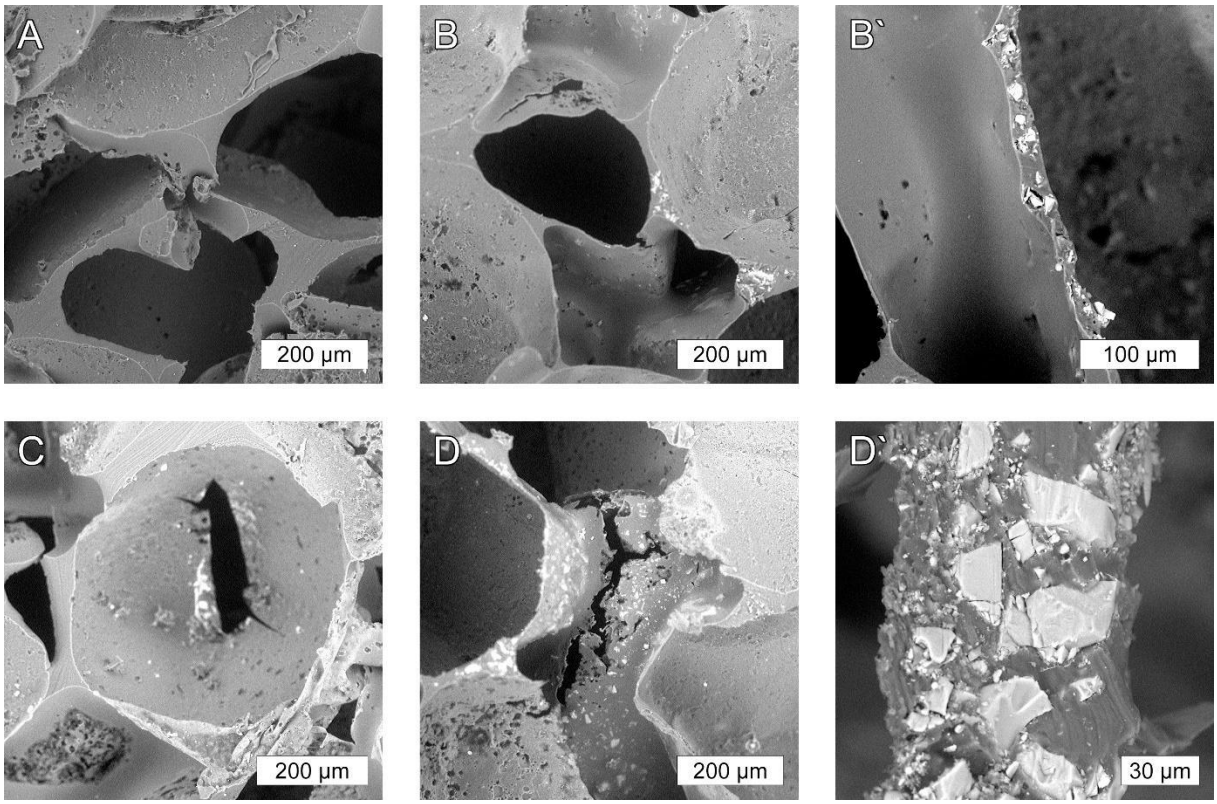


**Figure 4.** SEM images of foam scaffolds after compression tests A) PGA25, B) PGA25/BG, B` PGA25/BG walls, C) PGA50, D) PGA50/BG and D` PGA50/BG walls.

### Thermal properties of PGA scaffolds

Figure 5 contains DSC curves from the first and second heating cycles for PGA crosslinked at different LDI contents (Figure 5A), for PGA/BG composites crosslinked at different LDI contents (Figure 5B). As may be noticed, the glass transition temperature of PGA depends on the LDI content and whether or not there is bio-glass in the system. The lowest glass transition temperature values were obtained for PGA25. It is -19°C for the first heating scan and -9°C for the second heating scan (Figure 5A). In this case, slight changes in the glass transition temperature were noted when 20% by weight of bio-glass was added. Due to the stiffening of the polymer chains, there was a reduction to -21°C and -11°C for the first and second heating scans, respectively. Increasing the degree of cross-linking of PGA increases the glass transition temperature. Thus, for PGA50 values of -12 °C (first heating) and -2°C (second heating) were obtained. For PGA100, the highest glass transition temperatures were obtained

and are 18°C (first heating) and 25°C (second heating) (Figure 5B). For PGA50/BG and PGA100/BG, the addition of bio-glass also reduced $T_g$. For the PGA50/BG system, the addition of BG reduced $T_g$ by about 3°C (in both the first and second heating scans) relative to PGA50, while in the PGA100/TG composite, the reduction in $T_g$ is 10°C relative to the PGA100 reference (Figure 5B. For un-crosslinked PGA, glass transition temperatures range from -49°C to -34°C, depending on the synthesis temperature [10].

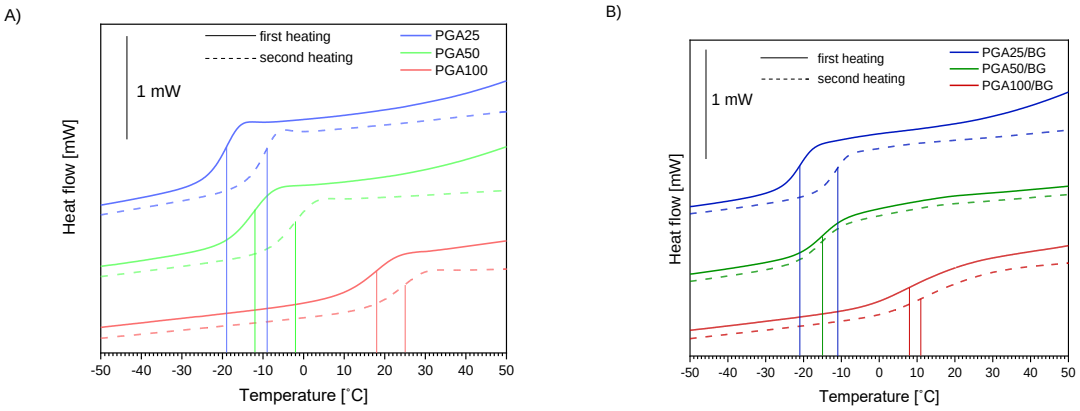


**Figure 5.** DSC first and second heating scan of foam scaffolds A) PGA25, PGA50 and PGA100, B) PGA25/BG, PGA50/BG and PGA100/BG

FTiR/ATR was used to confirm the different degree of PGA cross-linking depending on the LDI content. Figure 6 shows a slice of the FTiR/ATR spectra in the 3050-3800 $cm^{-1}$ range. The signal that comes from the hydroxyl stretching is in the range of 3500-3000 $cm^{-1}$. As the LDI content of the system increases, the signal shifts to lower wavelength values and decreases. The disappearance of the band originating from the hydroxyl stretching groups should be interpreted as the progress of the crosslinking reaction. In this case, it was confirmed that the cross-linking density is increasing in line with PGA25>PGA50>PGA100. In addition, it can be noted that PGAs containing bio-glass have lower peaks from hydroxyl groups than the corresponding unfilled polymers. This indicates that materials containing bio-glass are slightly better cross-linked than unfilled PGA.

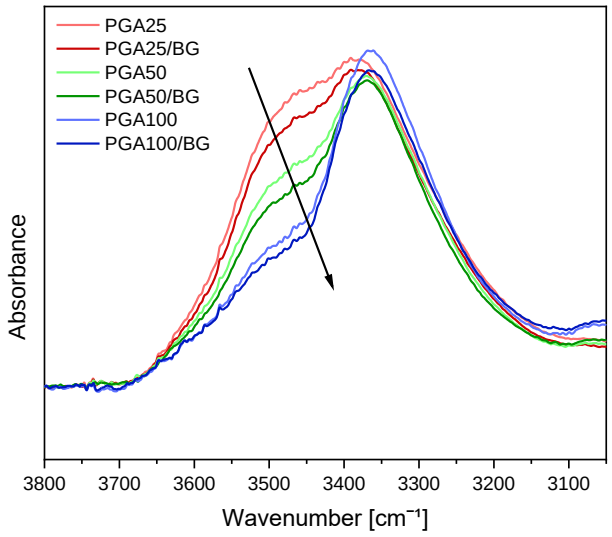


**Figure 6.** FTiR of PGA based sample

## Compression mechanical properties of PGA scaffolds

An important objective of the study was to investigate the behavior of the tested materials based on PGA crosslinked with different LDI content during compression testing. The samples were subjected to a quasi-static compression test, deforming it by 90%. It was noted that the content of LDI in the system is important in terms of strength properties. It was noted that increasing the content of the LDI crosslinking agent increases the strength parameters of the materials. For example, for a strain of 30%, 1.4kPA was obtained for PGA25, 2.0kPa was obtained for PGA50, and 3.3kPa was obtained for PGA100 (Table 3, Figure 7).

**Table 3**. Summary of compressive strength parameters for PGA/BG systems

| Sample | Compressive stress [kPa] | | |
|---|---|---|---|
| | at strain 30% | at strain 60% | at strain 90% |
| PGA25 | 1,4 +/- 0,2 | 7 +/- 1 | 440 +/- 30 |
| PGA25/BG | 1,6 +/- 0,2 | 7 +/- 1 | 460 +/- 30 |
| PGA50 | 2,0 +/- 0,2 | 9 +/- 1 | 450 +/- 50 |
| PGA50/BG | 2,7 +/- 0,2 | 14 +/- 1 | 700 +/- 30 |
| PGA100 | 3,3 +/- 0,2 | 20 +/- 2 | 1440 +/- 90 |
| PGA100/BG | 10,0 +/- 0,8 | 49 +/- 3 | 2130 +/- 90 |

Analogous observations were made for higher strain values. At the same time, the effect of bio-glass on mechanical properties was observed - systems with bio-glass additives are characterized by higher stresses relative to samples without bio-glass at the same strain and degree of crosslinking. The most notable differences are evident for PGA100, where 3.3kPA was obtained for a strain of 30%, while for PGA100/BG the stress value was 10kPA (Table 3).

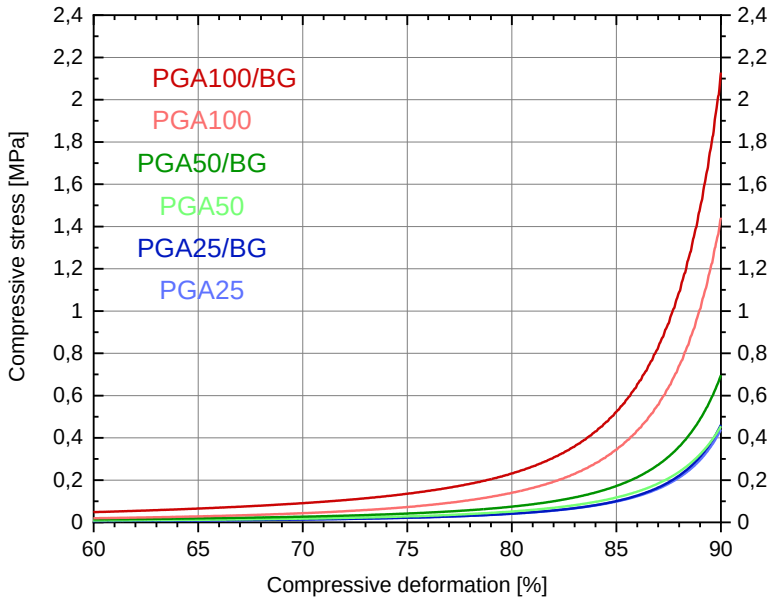


**Figure 7.** Compressive stress-strain plot for PGA and PGA/BG scaffolds

A detailed analysis was carried out for a 10-fold repetition of the compression test. The test was carried out as follows - the specimen was compressed up to 90% strain was reached, then the strain was relaxed and the 90% strain was set again, and the strain was measured. The results are shown graphically in Figure 8, and detailed data are summarized in Table 4 for strains of 30, 60 and 90%. The maximum values for PGA25 and PGA25/BG material were obtained at the highest strain of 90% and are 477kPa and 526kPa respectively. At the same time, the values of maximum stress at 90% strain after 10 cycles decreased for these samples to 89 and 94% respectively. The results indicate that the system with BG is less susceptible to mechanical failure as compared to the neat PGA25. The PGA50 and PGA100 samples were

similarly examined (Figure 8 B and C). For PGA50 and PGA50/BG at 90% strain, maximum stresses of 481 and 867kPa were obtained, respectively, while ~2.8MPa and ~3.2MPa were obtained for PGA100 and PGA100/BG materials respectively. After 10 cycles of compression, the values continued to be higher for the composites than for the pure PGAs, and for all materials the maximum values after 10 cycles of compression were at levels above 80% of the value obtained in the first compression,

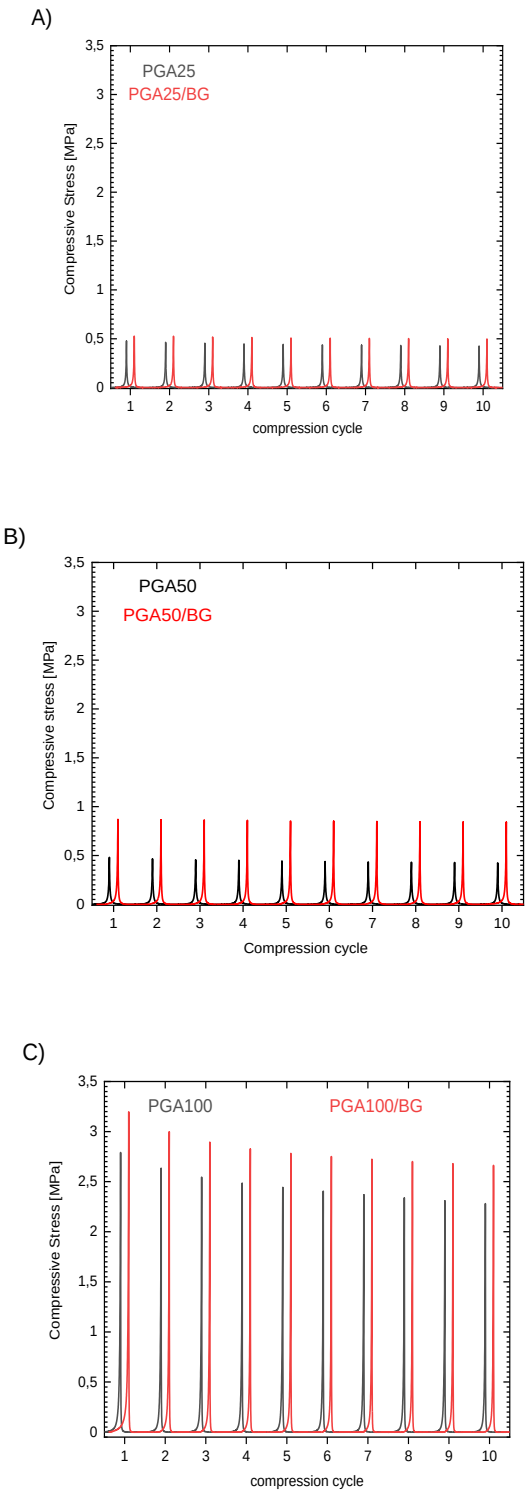


**Figure 8.** Stress-strain relationship for 10-fold deformation: a) PGA25 and PGA25/BG, b) PGA50 and PGA50/BG, c) PGA100 and PGA100/BG

**Table 4.** Summary of strength parameters at successive compression cycles

| strain 30% | | | | | | | | | | | |
|---|---|---|---|---|---|---|---|---|---|---|---|
| Sample | strain cycle I [kPa] | Strain change in the next cycle [%] | | | | | | | | | strain cycle X [kPa] |
| | | II | III | IV | V | VI | VII | VIII | IX | X | |
| PGA25 | 1,6 | 107,1 | 108,4 | 101,2 | 99,0 | 99,0 | 105,9 | 104,7 | 112,3 | 99,7 | 1,6 |
| PGA25/BG | 1,8 | 101,3 | 108,2 | 107,3 | 89,9 | 90,4 | 102,4 | 102,2 | 92,1 | 96,4 | 1,8 |
| PGA50 | 2,0 | 105,5 | 99,6 | 100,4 | 94,7 | 102,8 | 103,8 | 101,1 | 108,2 | 98,5 | 1,9 |
| PGA50/BG | 3,4 | 90,0 | 88,7 | 85,2 | 92,9 | 90,0 | 93,2 | 88,6 | 90,4 | 93,3 | 3,2 |
| PGA100 | 5,0 | 93,2 | 91,0 | 90,2 | 87,5 | 87,8 | 86,9 | 91,0 | 85,6 | 86,1 | 4,3 |
| PGA100/BG | 21,1 | 93,2 | 90,5 | 88,4 | 86,6 | 85,6 | 85,4 | 84,6 | 83,2 | 82,9 | 17,5 |
| strain 60% | | | | | | | | | | | |
| Sample | strain cycle I [kPa] | Strain change in the next cycle [%] | | | | | | | | | Strain Cycle X [kPa] |
| | | II | III | IV | V | VI | VII | VIII | IX | X | |
| PGA25 | 5,8 | 100,7 | 99,7 | 100,4 | 97,8 | 99,2 | 102,3 | 100,0 | 89,0 | 98,1 | 5,7 |
| PGA25/BG | 9,1 | 100,7 | 100,9 | 98,3 | 99,3 | 98,8 | 99,5 | 98,6 | 102,2 | 96,3 | 8,8 |
| PGA50 | 9,1 | 97,8 | 99,5 | 99,0 | 100,9 | 97,5 | 97,4 | 95,9 | 96,7 | 97,1 | 8,8 |
| PGA50/BG | 15,3 | 97,8 | 95,7 | 95,9 | 95,3 | 94,8 | 95,6 | 96,0 | 95,% | 93,9 | 14,4 |
| PGA100 | 30,6 | 95,6 | 95,3 | 94,8 | 95,3 | 93,6 | 94,6 | 95,0 | 94,6 | 95,0 | 29,1 |
| PGA100/BG | 73,5 | 94,4 | 91,6 | 89,6 | 88,6 | 87,9 | 87,0 | 86,0 | 85,8 | 85,1 | 62,6 |
| strain 90% | | | | | | | | | | | |
| Sample | strain cycle I [kPa] | Strain change in the next cycle [%] | | | | | | | | | Strain cycle X [kPa] |
| | | II | III | IV | V | VI | VII | VIII | IX | X | |
| PGA25 | 477 | 97,0 | 95,2 | 93,8 | 92,7 | 91,7 | 91,0 | 90,4 | 89,6 | 89,2 | 425 |
| PGA25/BG | 526 | 99,9 | 98,4 | 97,3 | 96,5 | 96,0 | 95,8 | 95,3 | 94,9 | 94,6 | 497 |
| PGA50 | 481 | 96,8 | 94,7 | 93,3 | 92,3 | 91,1 | 90,4 | 89,7 | 88,7 | 88,1 | 423 |
| PGA50/BG | 867 | 99,7 | 99,2 | 99,0 | 98,3 | 98,0 | 97,6 | 97,3 | 97,0 | 96,8 | 840 |
| PGA100 | 2791 | 94,3 | 91,1 | 88,9 | 87,4 | 86,2 | 84,8 | 83,8 | 82,6 | 81,6 | 2277 |
| PGA100/BG | 3195 | 93,7 | 90,6 | 88,4 | 87,0 | 86,0 | 85,2 | 84,4 | 83,8 | 83,3 | 2660 |

## Three-dimensional structure of PGA-based scaffolds

A comparative analysis of the structural parameters calculated before and after (10x) compression were conducted. The results are summarized in Table 5 (results before

compression) and in Table 6 (results after compression). 3D reconstructions of the tested materials are shown in Figure 9 and Figure 10. The conducted studies indicate that the structure of these samples before and after compression tests differ slightly. A slight decrease in the porosity of the samples was observed from a value of 0.25% (for sample PGA100) to 4% for sample PGA50. The porosity for all the samples is almost completely open (the content of closed pores for most samples is less than 0.001%). The applied loading increased the value of the major diameter value (Maj.Dm) by an average of 5%, with a concomitant decrease in the sphericity value of 0.29% for sample PGA50 to 12% for sample PGA25BG, respectively.

The obtained figures for the samples before and after 10-fold compression show very slight change in the basic parameters characterizing porosity. This is the main difference between the PLA-based scaffolds that have been studied most often. PLA materials are mostly rigid [41] and do not recover their shape after deformation.

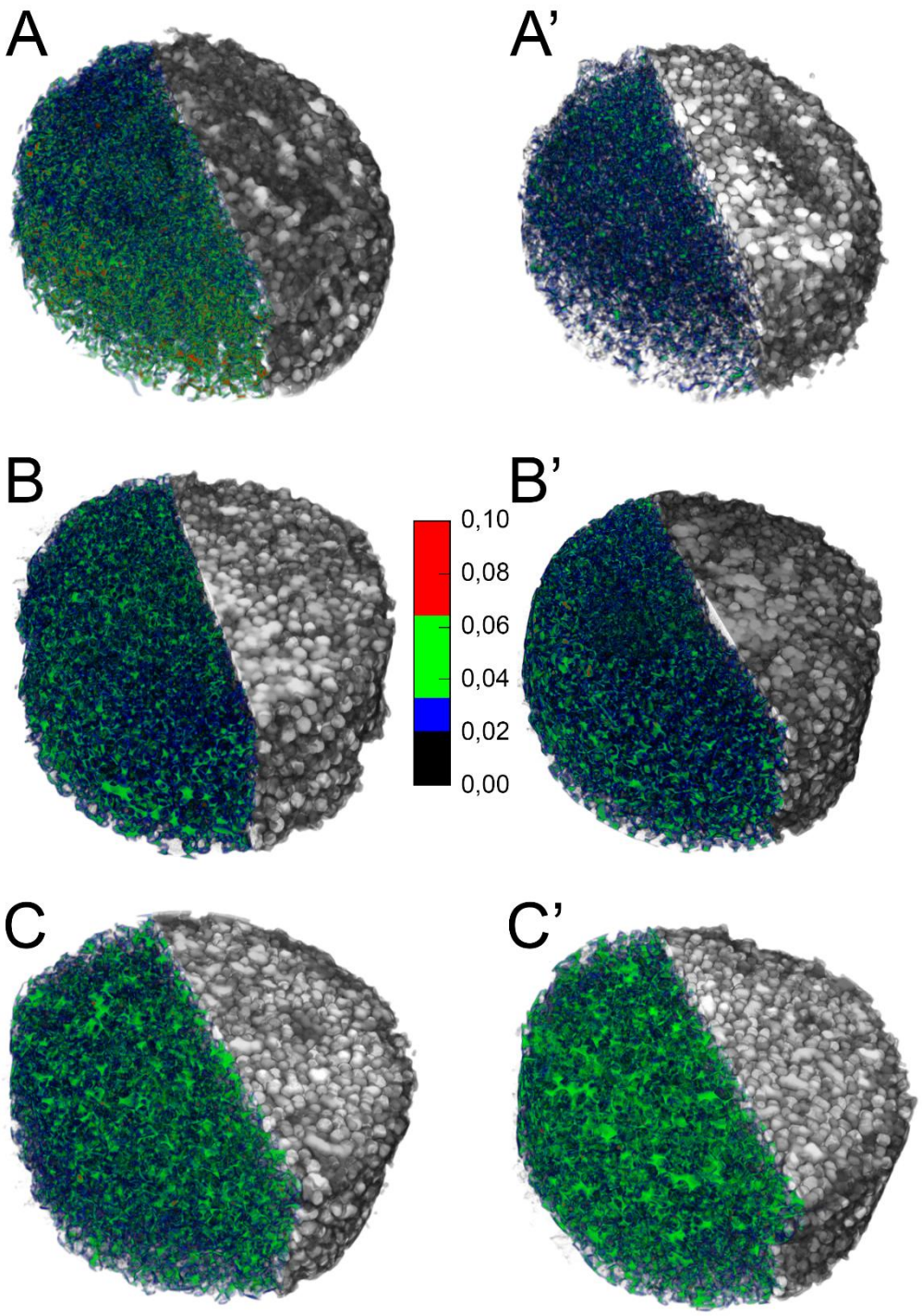


**Figure 9**. Three-dimentional reconstruction of scaffolds from CT scans **before** compression testing for: A) PGA25, A`)PGA25/BG, B) PGA50, B`) PGA50/BG, C) PGA100 and C`) PGA100/BG

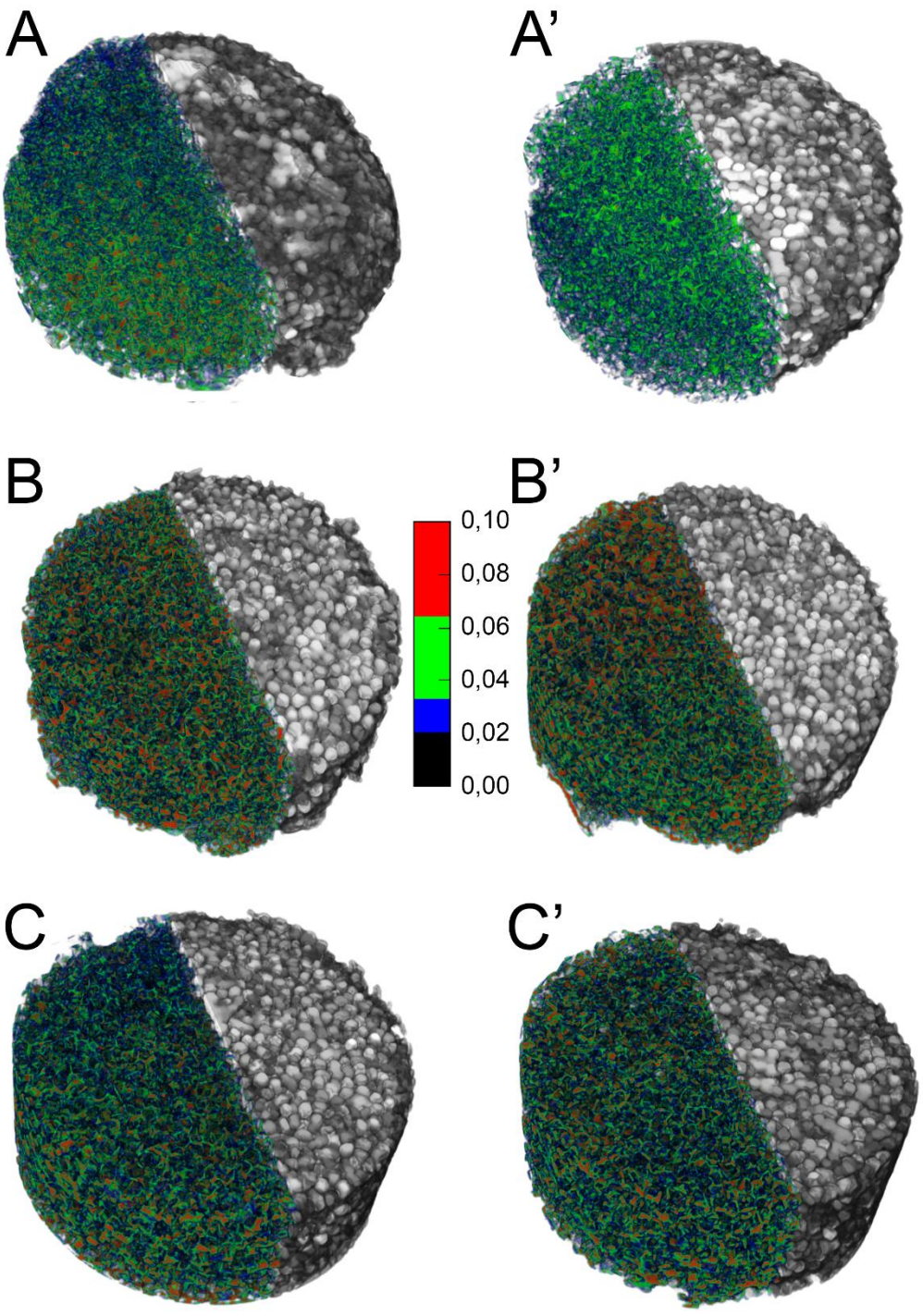


**Figure 10.** Three-dimentional reconstruction of scaffolds from CT scans **after 10x** compression testing for: A) PGA25, A`)PGA25/BG, B) PGA50, B`) PGA50/BG, C) PGA100 and C`) PGA100/BG

**Table 5.** Comparison of the values of structural parameters of samples **before** compression testing, determined in 3D structural measurements using CtAn software, Bruker

| | Po(tot)a [%] | Po(op)a [%] | Po(cl) a [%] | Po.V a [mm] | ESDv [um] | Maj.Dm [um] | Sp [-] | Sau.Dm [um] |
|---|---|---|---|---|---|---|---|---|
| PGA25 | 84,7 | 84,7 | <0,001 | 297,50 | 288,6±92 | 482,7±196 | 0,71±0,16 | 208,5±87 |
| PGA25BG | 80,7 | 80,7 | 0,005 | 283,18 | 297±99 | 487,9±232 | 0,72±0,16 | 218,4±89 |
| PGA50 | 75,8 | 75,8 | <0,001 | 240,80 | 384,4±138 | 542,2±276 | 0,81±0,12 | 305,4±83 |
| PGA50BG | 69,1 | 69,1 | 0,004 | 208,77 | 415,2±132 | 564,3±297 | 0,81±0,12 | 347,6±100 |
| PGA100 | 76,8 | 76,8 | 0,001 | 260,88 | 335,8±103 | 483,4±166 | 0,75±0,14 | 256,9±100 |
| PGA100BG | 72,7 | 72,7 | <0,001 | 246,65 | 350,1±200 | 539,7±243 | 0,75±0,13 | 275,2±108 |

[a]Parameters obtained from the 3D analysis; results shown as the mean value ± SD

**Table 6.** Comparison of the values of structural parameters of samples **after** compression testing, determined in 3D structural measurements using CtAn software, Bruker

| | Po(tot)a [%] | Po(op)a [%] | Po(cl) a [%] | Po.V [a] [mm] | ESDv [um] | Maj.Dm [um] | Sp [-] | Sau.Dm [um] |
|---|---|---|---|---|---|---|---|---|
| PGA25 | 83,9 | 83,9 | <0,001 | 294,47 | 283,2±104 | 528,0±258 | 0,66±0,17 | 190,5±89 |
| PGA25BG | 80,2 | 80,2 | 0,004 | 281,70 | 283,1±95 | 516,6±258 | 0,63±0,15 | 168,9±79 |
| PGA50 | 72,2 | 72,2 | <0,001 | 229,48 | 382,4±142 | 545,6±260 | 0,81±0,13 | 301,2±86 |
| PGA50BG | 63,6 | 63,6 | 0,001 | 227,07 | 404,5±140 | 593,1±321 | 0,79±0,12 | 321,4±103 |
| PGA100 | 76,7 | 76,7 | 0,001 | 260,27 | 329,1±99 | 506,8±190 | 0,71±0,14 | 221,3±99 |
| PGA100BG | 71,4 | 71,4 | <0,001 | 242,29 | 338,7±125 | 568,1±250 | 0,72±0,15 | 248,8±109 |

[a]Parameters obtained from the 3D analysis; results shown as the mean value ± SD

## 4. CONCLUSIONS

In this paper, we have presented the possibility of producing PGA and PGA-bioglass porous composites for bone tissue engineering. PGA prepolymer was obtained in enzymatic polymerization using *Candida Antarctica* enzyme in the first step of the research. L-lysine diisocyanate (LDI) was used as a cross-linking agent. LDI, apart from the cross-linking function, simultaneously introduces a bioactive component - L-lysine to the system in one process. Porous scaffolds were obtained using thermally induced phase separation combined with chemical cross-linking and salt leaching. We have demonstrated the possibility of tailoring

the properties of composite systems by changing the amount of LDI, which translates into a change in the PGA cross-linking density and also affects all the properties of the tested materials. The obtained PGA based materials are characterized by open porosity with porosity level of 85-90% and water sorption level between 710-850%. The obtained scaffolds were subjected to 10-fold compression with a strain of 90%. SEM analysis showed that in PGA-bioglass systems, no filler decohesion occurs after 10-fold compression. At the same time small cracks were observed in the walls of the material. Computer tomography (CT) showed little (up to few percent) changes between native samples and samples compressed 10 times. It was shown that the total porosity - Po(tot)a, as well as the open porosity - Po(op)a and pore volume - Po.V before and after compression, are at the same level. Slight changes were observed for major pore diameter (Maj.Dm) and sphericity (Sp). Major pore diameter increases after the compression process, while sphericity decreases regardless of whether the sample was PGA, PGA-bioglass, and what the degree of cross-linking was.

In this article, we have shown that it is possible to produce flexible polymer scaffolds based on PGA and bio-glass. The system was doped with LDI and this single compound served as a crosslinking, as well as a bioactive agent.

**Acknowledgment**

*The project entitled "Multifunctional composite materials with antimicrobial and pro-regenerative properties for use in bone surgery" is financed by The National Centre for Research and Development (Poland), project no. Techmatstrateg2/406384/7/NCBR/2019*

**Declaration of interests**

The authors declare that they have no known competing financial interests or personal relationships that could have appeared to influence the work reported in this paper.

## REFERENCES


[1] G.B. Perin, M.I. Felisberti, Enzymatic Synthesis of poly ( glycerol sebacate ): Kinetics , Chain Growth , and Branching Behavior . Polycondensation conditions and characteristics of glycerol-based polyesters prepared via CALB catalysis – A short review H- 13 C HSQC contour map synthe, (n.d.).

[2] S.M.E. Swainson, I.D. Styliari, V. Taresco, M.C. Garnett, Poly (glycerol adipate) (PGA), an Enzymatically Synthesized Functionalizable Polyester and Versatile Drug Delivery Carrier: A Literature Update, Polymers (Basel). 11 (2019) 1561. https://doi.org/10.3390/polym11101561.

[3] P. Piszko, B. Kryszak, A. Piszko, K. Szustakiewicz, Brief review on poly(glycerol sebacate) as an emerging polyester in biomedical application: Structure, properties and modifications, Polim. Med. 51 (2021) 43–50. https://doi.org/10.17219/pim/139585.

[4] S.M.E. Swainson, V. Taresco, A.K. Pearce, L.H. Clapp, B. Ager, M. McAllister, C. Bosquillon, M.C. Garnett, Exploring the enzymatic degradation of poly(glycerol adipate), Eur. J. Pharm. Biopharm. 142 (2019) 377–386. https://doi.org/10.1016/j.ejpb.2019.07.015.

[5] A.S. Kulshrestha, W. Gao, R.A. Gross, Glycerol copolyesters: Control of branching and molecular weight using a lipase catalyst, Macromolecules. 38 (2005) 3193–3204. https://doi.org/10.1021/ma0480190.

[6] T. Wersig, R. Krombholz, C. Janich, A. Meister, J. Kressler, K. Mäder, Indomethacin

functionalised poly(glycerol adipate) nanospheres as promising candidates for modified drug release, Eur. J. Pharm. Sci. 123 (2018) 350–361. https://doi.org/10.1016/j.ejps.2018.07.053.

[7] A. Zamboulis, E.A. Nakiou, E. Christodoulou, D.N. Bikiaris, E. Kontonasaki, L. Liverani, A.R. Boccaccini, Polyglycerol hyperbranched polyesters: Synthesis, properties and pharmaceutical and biomedical applications, Int. J. Mol. Sci. 20 (2019). https://doi.org/10.3390/ijms20246210.

[8] S. Puri, P. Kallinteri, S. Higgins, G.A. Hutcheon, M.C. Garnett, Drug incorporation and release of water soluble drugs from novel functionalised poly(glycerol adipate) nanoparticles, J. Control. Release. 125 (2008) 59–67. https://doi.org/10.1016/j.jconrel.2007.09.009.

[9] B.J. Kline, E.J. Beckman, A.J. Russell, One-step biocatalytic synthesis of linear polyesters with pendant hydroxyl groups, J. Am. Chem. Soc. 120 (1998) 9475–9480. https://doi.org/10.1021/ja9808907.

[10] V. Taresco, R.G. Creasey, J. Kennon, G. Mantovani, C. Alexander, J.C. Burley, M.C. Garnett, Variation in structure and properties of poly(glycerol adipate) via control of chain branching during enzymatic synthesis, Polym. (United Kingdom). 89 (2016) 41–49. https://doi.org/10.1016/j.polymer.2016.02.036.

[11] P.L. Jacob, L.A. Ruiz Cantu, A.K. Pearce, Y. He, J.C. Lentz, J.C. Moore, F. Machado, G. Rivers, E. Apebende, M.R. Fernandez, I. Francolini, R. Wildman, S.M. Howdle, V. Taresco, Poly (glycerol adipate) (PGA) backbone modifications with a library of functional diols: Chemical and physical effects, Polymer (Guildf). 228 (2021) 123912. https://doi.org/10.1016/j.polymer.2021.123912.

[12] D. Sagnelli, R. Cavanagh, J. Xu, S.M.E. Swainson, A. Blennow, J. Duncan, V. Taresco, S. Howdle, Starch/poly (glycerol-adipate) nanocomposite film as novel biocompatible materials, Coatings. 9 (2019) 482. https://doi.org/10.3390/coatings9080482.

[13] V. Taresco, J. Suksiriworapong, R. Creasey, J.C. Burley, G. Mantovani, C. Alexander, K. Treacher, J. Booth, M.C. Garnett, Properties of Acyl Modified Poly ( Glycerol-Adipate ) Comb-Like Polymers and Their Self-Assembly into Nanoparticles, (2016) 3267–3278. https://doi.org/10.1002/pola.28215.

[14] P. Kallinteri, S. Higgins, G.A. Hutcheon, C.B. St. Pourçain, M.C. Garnett, Novel functionalized biodegradable polymers for nanoparticle drug delivery systems, Biomacromolecules. 6 (2005) 1885–1894. https://doi.org/10.1021/bm049200j.

[15] R.H. Argent, S.M.E. Swainson, J. Booth, E. Turpin, C.A. Laughton, J.C. Burley, M.C. Garnett, RSC Advances, (2016) 109401–109405. https://doi.org/10.1039/c6ra21464a.

[16] J. Suksiriworapong, V. Taresco, D.P. Ivanov, I.D. Styliari, K. Sakchaisri, V. Buraphacheep, M.C. Garnett, Colloids and Surfaces B : Biointerfaces Synthesis and properties of a biodegradable polymer-drug conjugate : Methotrexate-poly ( glycerol adipate ), Colloids Surfaces B Biointerfaces. 167 (2018) 115–125. https://doi.org/10.1016/j.colsurfb.2018.03.048.

[17] A. Gregor, E. Filová, M. Novák, J. Kronek, H. Chlup, M. Buzgo, V. Blahnová, V. Lukášová, M. Bartoš, A. Nečas, J. Hošek, Designing of PLA scaffolds for bone tissue replacement fabricated by ordinary commercial 3D printer, J. Biol. Eng. 11 (2017). https://doi.org/10.1186/s13036-017-0074-3.

[18] K. Rodríguez, S. Renneckar, P. Gatenholm, Biomimetic Calcium Phosphate Crystal

Mineralization on Electrospun Cellulose-Based Scaffolds, ACS Appl. Mater. Interfaces. 3 (2011) 681–689. https://doi.org/10.1021/am100972r.

[19] S. Lee, M.K. Joshi, A.P. Tiwari, B. Maharjan, K.S. Kim, Y.H. Yun, C.H. Park, C.S. Kim, Lactic acid assisted fabrication of bioactive three-dimensional PLLA/B-TCP fibrous scaffold for biomedical application, Chem. Eng. J. 347 (2018) 771–781. https://doi.org/10.1016/j.cej.2018.04.158.

[20] Y. Wang, Y. Gao, G. Xu, H. Liu, Y. Xiang, W. Cui, Accelerated fabrication of antibacterial and osteoinductive electrospun fibrous scaffolds: Via electrochemical deposition, RSC Adv. 8 (2018) 9546–9554. https://doi.org/10.1039/c8ra01011k.

[21] M. Mehrabanian, M. Nasr-Esfahani, HA/nylon 6,6 porous scaffolds fabricated by salt-leaching/solvent casting technique: effect of nano-sized filler content on scaffold properties., Int. J. Nanomedicine. 6 (2011) 1651–1659.

[22] M. Singh, B. Sandhu, A. Scurto, C. Berkland, M.S. Detamore, Acta Biomaterialia Microsphere-based scaffolds for cartilage tissue engineering : Using subcritical CO 2 as a sintering agent q, Acta Biomater. 6 (2010) 137–143. https://doi.org/10.1016/j.actbio.2009.07.042.

[23] Y.J. Seol, T.Y. Kang, D.W. Cho, Solid freeform fabrication technology applied to tissue engineering with various biomaterials, Soft Matter. 8 (2012) 1730–1735. https://doi.org/10.1039/c1sm06863f.

[24] M.G. Gandolfi, F. Zamparini, M. Degli Esposti, F. Chiellini, F. Fava, P. Fabbri, P. Taddei, C. Prati, Highly porous polycaprolactone scaffolds doped with calcium silicate and dicalcium phosphate dihydrate designed for bone regeneration, Mater. Sci. Eng. C. 102 (2019) 341–361. https://doi.org/10.1016/j.msec.2019.04.040.

[25] S.S. Lee, X. Du, T. Smit, E.G. Bissacco, D. Seiler, M. De Wild, S.J. Ferguson, Biomaterials Advances 3D-printed LEGO ® -inspired titanium scaffolds for patient-specific regenerative medicine, Biomater. Adv. 154 (2023) 213617. https://doi.org/10.1016/j.bioadv.2023.213617.

[26] P. Singh, H. Baniasadi, S. Gupta, R. Ghosh, S. Shaikh, International Journal of Biological Macromolecules 3D-printed cellulose nanocrystals and gelatin scaffolds with bioactive cues for regenerative medicine : Advancing biomedical applications, 278 (2024). https://doi.org/10.1016/j.ijbiomac.2024.134402.

[27] X. He, R. Wang, F. Zhou, H. Liu, International Journal of Biological Macromolecules Recent advances in photo-crosslinkable methacrylated silk ( Sil-MA ) -based scaffolds for regenerative medicine : A review, 256 (2024). https://doi.org/10.1016/j.ijbiomac.2023.128031.

[28] R. Akbarzadeh, A.-M. Yousefi, Effects of processing parameters in thermally induced phase separation technique on porous architecture of scaffolds for bone tissue engineering Effects of processing parameters in thermally induced phase separa- tion technique on porous architecture of s, J Biomed Mater Res Part B Appl Bio-Mater J Biomed Mater Res Part B. 102102 (2014). https://doi.org/10.1002/jbm.b.33101.

[29] K. Szustakiewicz, M. Włodarczyk, M. Gazińska, K. Rudnicka, P. Płociński, P. Szymczyk-Ziółkowska, G. Ziółkowski, M. Biernat, K. Sieja, M. Grzymajło, P. Jóźwiak, S. Michlewska, A.. Trochimczuk, The Effect of Pore Size Distribution and L - Lysine Modified Apatite Whiskers ( HAP ) on Osteoblasts Response in PLLA / HAP foam Scaffolds Obtained in the Thermally Induced Phase Separation Process, Int. J. Mol. Sci. (2021).

[30] K. Szustakiewicz, M. Gazińska, B. Kryszak, M. Grzymajło, J. Pigłowski, R.J. Wiglusz, M. Okamoto, The influence of hydroxyapatite content on properties of poly(L-lactide)/hydroxyapatite porous scaffolds obtained using thermal induced phase separation technique, Eur. Polym. J. 113 (2019). https://doi.org/10.1016/j.eurpolymj.2019.01.073.

[31] P. Piszko, M. Włodarczyk, S. Zielińska, M. Gazińska, P. Płociński, K. Rudnicka, A. Szwed, A. Krupa, M. Grzymajło, A. Sobczak-Kupiec, D. Słota, M. Kobielarz, M. Wojtków, K. Szustakiewicz, PGS/HAp microporous composite scaffold obtained in the TIPS-TCL-SL method: An innovation for bone tissue engineering, Int. J. Mol. Sci. 22 (2021). https://doi.org/10.3390/ijms22168587.

[32] Z. Wang, Y. Ma, Y.X. Wang, Y. Liu, K. Chen, Z. Wu, S. Yu, Y. Yuan, C. Liu, Urethane-based low-temperature curing, highly-customized and multifunctional poly(glycerol sebacate)-co-poly(ethylene glycol) copolymers, Acta Biomater. 71 (2018) 279–292. https://doi.org/10.1016/j.actbio.2018.03.011.

[33] V. Hevilla, A. Sonseca, C. Echeverría, A. Muñoz-Bonilla, M. Fernández-García, Photocuring of aliphatic-lineal poly(glycerol adipate) with a monomer bearing thiazolium groups as a promising approach for biomedical applications, Eur. Polym. J. 186 (2023). https://doi.org/10.1016/j.eurpolymj.2023.111875.

[34] S. Jalota, S.B. Bhaduri, A.C. Tas, In vitro testing of calcium phosphate (HA, TCP, and biphasic HA-TCP) whiskers, J. Biomed. Mater. Res. Part A. 78A (2006) 481–490. https://doi.org/10.1002/jbm.a.30851.

[35] Y. Li, Y. Wang, Y. Li, W. Luo, J. Jiang, J. Zhao, C. Liu, Controllable Synthesis of Biomimetic Hydroxyapatite Nanorods with High Osteogenic Bioactivity, ACS

Biomater. Sci. Eng. 6 (2020) 320–328. https://doi.org/10.1021/acsbiomaterials.9b00914.

[36] C.C. Lau, M. Al Qaysi, N. Owji, M.K. Bayazit, J. Xie, J.C. Knowles, J. Tang, Advanced biocomposites of poly(glycerol sebacate) and β-tricalcium phosphate by in situ microwave synthesis for bioapplication, Mater. Today Adv. 5 (2020). https://doi.org/10.1016/j.mtadv.2019.100023.

[37] M. Fini, P. Torricelli, G. Giavaresi, A. Carpi, A. Nicolini, R. Giardino, Effect of L-lysine and L-arginine on primary osteoblast cultures from normal and osteopenic rats, Biomed. Pharmacother. 55 (2001) 213–220. https://doi.org/10.1016/S0753-3322(01)00054-3.

[38] M. Gazińska, A. Krokos, M. Kobielarz, M. Włodarczyk, P. Skibińska, B. Stępak, A. Antończak, M. Morawiak, P. Płociński, K. Rudnicka, Influence of hydroxyapatite surface functionalization on thermal and biological properties of poly(L-lactide)-and poly(l-lactide-co-glycolide)-based composites, Int. J. Mol. Sci. 21 (2020) 1–21. https://doi.org/10.3390/ijms21186711.

[39] A. Korbut, M. Włodarczyk, K. Rudnicka, A. Szwed, P. Płociński, M. Biernat, P. Tymowicz-Grzyb, M. Michalska, N. Karska, S. Rodziewicz-Motowidło, K. Szustakiewicz, Three component composite scaffolds based on PCL, hydroxyapatite, and l-lysine obtained in TIPS-SL: Bioactive material for bone tissue engineering, Int. J. Mol. Sci. 22 (2021). https://doi.org/10.3390/ijms222413589.

[40] L. Ciołek, M. Krok-Borkowicz, A. Gąsiński, M. Biernat, A. Antosik, E. Pamuła, Bioactive Glasses Enriched with Strontium or Zinc with Different Degrees of Structural Order as Components of Chitosan-Based Composite Scaffolds for Bone

Tissue Engineering, Polymers (Basel). 15 (2023). https://doi.org/10.3390/polym15193994.

[41] Ö.C. Önder, E. Yilgör, I. Yilgör, Fabrication of rigid poly(lactic acid) foams via thermally induced phase separation, Polymer (Guildf). 107 (2016) 240–248. https://doi.org/10.1016/j.polymer.2016.11.025.